Structural Forces in Self-Assembled Monolayers: Terphenyl-Substituted Alkanethiols on Noble Metal Substrates†

A. Shaporenko,‡ M. Brunnbauer,§ A. Terfort,*,§ M. Grunze,‡ and M. Zharnikov*,‡

Angewandte Physikalische Chemie, Universität Heidelberg, Im Neuenheimer Feld 253, 69120 Heidelberg, Germany, and Anorganische und Angewandte Chemie, Universität Hamburg, 20146 Hamburg, Germany

Received: January 22, 2004; In Final Form: April 19, 2004

Self-assembled monolayers (SAMs) formed from 4,4′-terphenyl-substituted alkanethiols $C_6H_5(C_6H_4)_2(CH_2)_n$-SH (TP*n*, $n = 1-6$) on polycrystalline (111) gold and silver substrates have been characterized by X-ray photoelectron spectroscopy (XPS), high-resolution XPS, near-edge X-ray absorption fine structure spectroscopy, ellipsometry, and water contact angle measurements. The packing density of the SAM constituents and the orientation of the terphenyl moieties exhibited a pronounced odd−even variation with the number (*n*) of methylene groups in the aliphatic $(CH_2)_n$ linker, which was opposite on silver as compared to gold. A higher packing density and a corresponding smaller inclination of the terphenyl moieties was observed for odd numbers of the methylene units in TP*n* on Au, and for even numbers of these units in TP*n* on Ag. The observed odd−even effects are explained by the strong dependence of the bending potentials in the metal−S−C bond on the deviation of the metal−S−C bond angle from an optimal value of ≈104° (Au) and ≈180° (Ag), respectively. The optimal metal−S−C angles are determined by the hybridization of the sulfur in the metal−thiolate bond, which is proposed to have sp^3 hybridization on Au and an sp hybridization on Ag, respectively.

1. Introduction

Self-assembled monolayers (SAMs) are 2D polycrystalline films of semirigid molecules that are chemically anchored to a suitable substrate. During the last two decades these systems attracted considerable attention because they allow the preparation of organic surfaces with a specific chemical identity and provide a means to tailor surfaces properties such as wetting, adhesion, lubrication, corrosion, and biocompatibility.[1−4] In addition, these assemblies can also be used to prepare micro- and nanostructured substrates for sensor applications and for fundamental studies on the interaction of proteins and cells with artificial surfaces.

Depending on the application, different SAMs can be fabricated following a building block scheme combining suitable chemical groups as a SAM constituent: a headgroup that binds strongly to the substrate, a tail group that constitutes the outer surface of the film, and a spacer that separates head and tail groups. At a given chemical composition of the SAM constituents, the properties of a SAM depend on its structure and packing density. These, in turn, result from the complex interplay of intermolecular and headgroup−substrate interactions, provided that the tail groups are weakly interacting.[5]

As an example for the interplay of structural forces, SAMs of ω-substituted alkanethiolates (AT) on gold and silver can be considered; these films are probably the best studied SAM systems due to their stability and the easiness of fabrication (see, e.g., refs 3, 4, and 6−8). Whereas the van der Waals interaction between the aliphatic chains are the major driving force for self-assembly in these systems, the packing of the AT chains is believed to be strongly affected by a corrugation of the sulfur−metal binding energy surface.[1−3,9] In the case of Ag, this corrugation is rather weak, which allows a dense packing of AT chains in a $(\sqrt{7}\times\sqrt{7})$R19.1° incommensurate structure with a lattice constant of ≈4.67−4.77 Å, close to the next neighbor distance in bulk paraffin crystals (≈4.4 Å).[2,4,10−12] In the case of Au, the corrugation of the sulfur−metal potential is assumed to be more pronounced,[9] which results in formation of a nearly commensurate c(4×2)-modulated $(\sqrt{3}\times\sqrt{3})$R30° lattice superstructure, with a larger intermolecular spacing of ≈5.0 Å.[2,4,10,13,14] In this lattice, minimization of energy is achieved by tilting of the AT molecules by ≈30° (the tilt angle depends on the experimental technique used[15]),[7,8,13] which is noticeably larger than the tilt in the AT/Ag systems (10−12°).[8,11]

Whereas this model gives a simple and self-consistent explanation of the observed arrangement of the AT moieties, there is an additional important factor, which is the character and geometry of the headgroup−substrate interaction. Supported by different experimental data, an sp^3 bonding configuration of the chemisorbed sulfur headgroup on Au(111) and sp bonding on Ag(111) associated with surface−S−C angles of ≈104° and ≈180°, respectively, were proposed.[8,16−20] Using model systems of semifluorinated and biphenyl-substituted ATs, it was shown that the hybridization and hence spatial orientation of the sulfur bonding orbitals is crucial for the orientation and packing density in the AT SAMs on Au and Ag substrates.[17−20] In particular, in biphenyl-substituted alkanethiols $CH_3(C_6H_4)_2(CH_2)_n$SH (BPn), the orientation and the packing density of the rigid and strongly interacting biphenyl moieties was found to be directly dependent on the length of the short ($n = 1-6$) aliphatic spacer, so that a more upright orientation and a higher packing density were observed for an odd number of methylene units on Au and an even number on Ag.[17,19,21] This behavior could only be explained assuming an all-trans conformation of alkyl chain and rigid metal−S−C angles close to 104° (sp^3) and 180° (sp) for Au

† Part of the special issue "Gerhard Ertl Festschrift".

* Corresponding authors. M.Z.: e-mail, Michael.Zharnikov@urz.uni-heidelberg.de. A.T. e-mail, aterfort@xray.chemie.uni-hamburg.de.

‡ Universität Heidelberg.

§ Universität Hamburg.

10.1021/jp0400521 CCC: $27.50 © 2004 American Chemical Society
Published on Web 08/04/2004

and Ag, respectively. The minimization of the energy is achieved by the respective hybridization of the sulfur atom, rather than by a closer packing of the biphenyl moieties, which could require the distortion of the metal−S−C angle.

In this study, we further evaluate the importance of the spatial orientation of the sulfur bonding orbitals for the structure and packing density in alkanethiolate self-assembled monolayers. To increase the possible energy gain by forming dense molecular arrangements, we used terphenyl tail groups and studied the SAMs of 4,4′-terphenyl-substituted alkanethiols $C_6H_5(C_6H_4)_2(CH_2)_nSH$ (TP*n*, $n = 1-6$) on gold and silver substrates. For the characterization of the films, several complementary experimental techniques, such as X-ray photoelectron spectroscopy (XPS), high-resolution XPS (HRXPS), near-edge X-ray absorption fine structure (NEXAFS) spectroscopy, ellipsometry, and contact angle measurements were applied.

Note that only few studies on TP*n* SAMs have been published so far, in which TP1,[22−28] TP2,[28] and TP3[24,28] on Au have been considered. These studies were mostly concerned with either the comparison of TP*n* films with pure aromatic SAMs or electrical conduction of TP*n* molecules, and did not put a special emphasis on the bonding geometry of the thiolate headgroup. In the following section we describe the experimental procedure and techniques. The results are presented and briefly discussed in section 3. An extended analysis of the data is given in section 4, followed by a summary in section 5.

2. Experimental Section

The synthesis of the TP*n* compounds is described elsewhere.[24,28−30] The gold and silver substrates were prepared by thermal evaporation of 200 nm of gold or 100 nm of silver (99.99% purity) onto polished single-crystal silicon (100) wafers (Silicon Sense) primed with a 5 nm titanium adhesion layer. The resulting metal films are polycrystalline, with a grain size of 20−50 nm as observed by atomic force microscopy. The grains predominantly exhibit an (111) orientation, which is also corroborated by the angular distributions of the Au 4f photoelectrons[31] and by the characteristic binding energy (BE) shift of the Au 4f surface core level.[32] The SAMs were prepared by immersion of the freshly prepared substrates into a 1 mM TP*n* solution in THF at room temperature for 24 h. After immersion, the samples were carefully rinsed with pure solvent and blown dry with argon. No evidence for impurities or oxidative degradation products was found in the XPS and NEXAFS spectra.

For comparison, SAMs of 1,1′;4′,1″-terphenyl-4-thiols (TPT: $C_6H_5(C_6H_4)_2SH$) and hexadecanethiol (C16: $CH_3(CH_2)_{15}SH$) were fabricated using the same film preparation procedure as for the TP*n* SAMs. In the case of C16, absolute ethanol was used as a solvent.

The organic monolayers were characterized by XPS, HRXPS, NEXAFS spectroscopy, ellipsometry, and contact angle measurements. All experiments were performed at room temperature. The XPS, HRXPS, and NEXAFS spectroscopy measurements were carried out under UHV conditions at a base pressure $<1.5 \times 10^{-9}$ mbar. The time for these measurements was selected as a compromise between spectra quality and damage induced by X-rays.[33−36]

The XPS measurements were performed using two different spectrometers equipped with a Mg Kα X-ray source and either a VG CLAM 2 or LHS11 analyzer. In both cases, the spectra acquisition was carried out in normal emission geometry with an energy resolution of ≈0.9 eV. The X-ray sources were operated at 260 W power and positioned ≈1 cm away from the samples. The energy scale was referenced to the Au $4f_{7/2}$ peak at a binding energy (BE) of 84.0 eV.[37] For each sample, a wide scan spectrum and the C 1s, O 1s, S 2p, and Au 4f or Ag 3d narrow scan spectra were measured. The narrow scan spectra for the different samples were normalized to the integral intensity of the respective wide scan spectrum to correct for small differences in sample positions and X-ray source intensities.[18]

The HRXPS experiments were performed at the bending magnet beamline D1011 at the MAX II storage ring of the MAX-lab synchrotron radiation facility in Lund, Sweden. The HRXPS spectra were acquired in normal emission geometry at photon energies of 350 and 580 eV for the C 1s range and 350 eV for the S 2p region, respectively. The energy resolution was better than 100 meV. Every spectrum was individually calibrated using the Au $4f_{7/2}$ emission line of a *n*-alkanethiolate covered Au substrate at 83.93 eV,[32] which was identical to the XPS calibration to 84.0 eV considering a slight upward shift of the Au $4f_{7/2}$ bulk component for clean Au.[32] The value 83.93 eV was obtained by a separate calibration to the Fermi edge of a clean Pt-foil.[32]

Both XPS and HRXPS spectra were fitted by symmetric Voigt functions and a Shirley-type background. To fit the S $2p_{3/2,1/2}$ doublet we used two peaks with the same full width at half-maximum (fwhm), the standard[37] spin−orbit splitting of ≈1.18 eV (verified by fit), and a branching ratio of 2 ($S2p_{3/2}$/$S2p_{1/2}$). The fits were performed self-consistently: the same fit parameters were used for identical spectral regions.

The NEXAFS measurements were performed at the HE-SGM beamline of the synchrotron storage ring BESSY II in Berlin, Germany. The spectral acquisition was carried out at the carbon K-edge in the partial electron yield mode with a retarding voltage of −150 V. Linear polarized synchrotron light with a polarization factor of ≈82% was used. The energy resolution was ≈0.40 eV. The incidence angle of the light was varied from 90° (**E**-vector in the surface plane) to 20° (**E**-vector nearly normal to the surface) in steps of 10°-20° to monitor the orientational order of the TP*n* molecules within the films. This approach is based on the linear dichroism in X-ray absorption, i.e., the strong dependence of the cross-section of the resonant photoexcitation process on the orientation of the electric field vector of the linearly polarized light with respect to the molecular orbital of interest.[38]

The raw NEXAFS spectra were normalized to the incident photon flux by division through a spectrum of a clean, freshly sputtered gold sample. In the case of the Ag substrate, a spectrum of clean silver was subtracted from the raw spectrum of a SAM sample before normalization.[18,39] The energy scale was referenced to the pronounced π_1^* resonance of highly oriented pyrolytic graphite (HOPG) at 285.38 eV.[40]

The ellipsometry measurements were carried out usingthe M-44 ellipsometer of J. A. Woollam Co. Inc. The data were analyzed with the respective software. The incident angle was set to 75° and calibrated with a silicon wafer as a reference. A refractive index of 1.47 was assumed for all films in the calculation of their thickness.[41]

Infrared absorption measurements were performed with a dry-air-purged Bio-Rad FTIR spectrometer Model FTS 175C equipped with a liquid nitrogen cooled MCT detector. All spectra were taken using p-polarized light incident at a fixed angle of 80° with respect to the surface normal. The spectra were measured at a resolution of 2 cm^{-1} and are reported in absorbance units $A = -\log R/R_0$, where R is the reflectivity of the substrate with the monolayer and R_0 is the reflectivity of

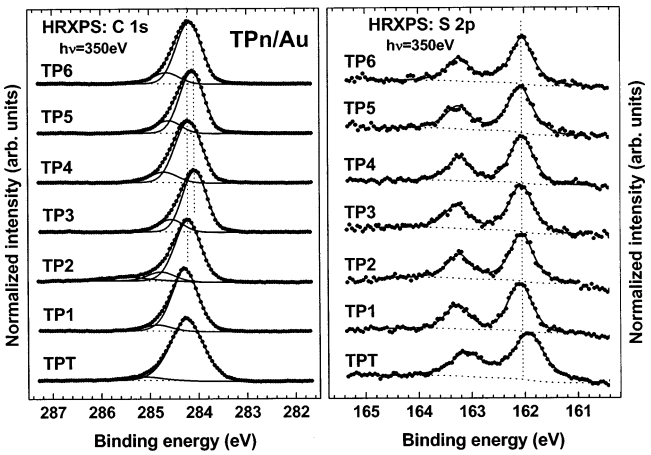

Figure 1. Normalized C 1s (left panel) and S 2p (right panel) HRXPS spectra of TP*n*/Au acquired at a photon energy of 350 eV. The fits of the C 1s peak and the higher BE shoulder are also shown.

the reference. Substrates covered with a SAM of perdeuterated hexadecanethiol were used as a reference.

Advancing contact angles of Millipore water were measured on freshly prepared samples with a Krüss goniometer Model G1. The measurements were performed under ambient conditions with the needle tip in contact with the drop. At least three measurements at different locations on each sample were made. The averaged values are reported. Deviations from the average were less than ±1°.

3. Results

3.1. XPS and HRXPS. Both XRS and HRXPS data suggest the formation of contamination-free, densely packed TP*n* films on Au and Ag. As an example, C 1s and S 2p HRXPS spectra of TP*n*/Au acquired at a PE of 350 eV are presented in Figure 1. All S 2p spectra exhibit a single S $2p_{3/2,1/2}$ doublet commonly assigned to the thiolate-type sulfur bonded to the metal surfaces.[8,32] The C 1s spectra show a main emission peak at a BE of 284.1−284.2 eV assigned to the aromatic backbone and a shoulder at ≈0.6 eV higher BE. Similar shoulders were observed previously for different aromatic SAMs and alternatively assigned to the carbon atom bonded to the sulfur headgroup or to shake-up processes.[42−46] As the probing depth of HRXPS is rather small at the given photon energy, the former assignment seems to be rather questionable and an assignment to a shake-up process is more likely.[47]

Whereas the spectra in Figure 1 are normalized to the maximum intensity, the nonnormalized spectra exhibit pronounced intensity variation. In the case of the C 1s spectra, this intensity variation can be directly used to monitor the effective film thickness. The latter parameter was calculated from the XPS data using a standard expression for an exponential attenuation of the XPS signal and an attenuation length of 31, 27, and 25.7 Å for the Au 4f, C 1s, and Ag 3d emissions, respectively.[15,45] The derived film thicknesses are presented in Figure 2. Apart from the general increase of the effective thickness with increasing length of the aliphatic chain, there are pronounced zigzag deviations from the general trend at a level of ±5−7%. The observed zigzag changes are inverse for Au and Ag substrates; i.e., a higher effective thickness is observed for an odd number of the methylene units in TP*n*/Au and an even number of these entities in TP*n*/Ag.

3.2. Ellipsometry. The effective thickness of the TP*n* films derived from the ellipsometry measurements is presented in Figure 3. Apart from the somewhat higher values in the case of

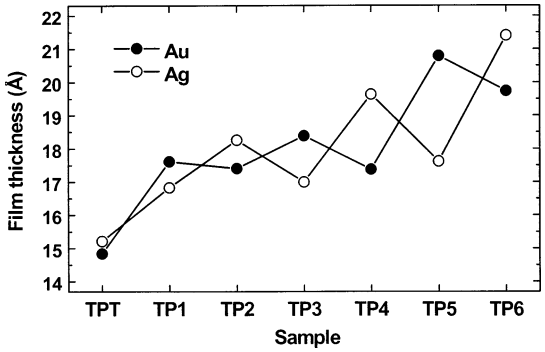

Figure 2. Effective thickness of TP*n*/Au (full circles) and TP*n*/Ag (hollow circles) derived from the XPS data (C1s/Au4f and C1s/Ag3d intensity ratios).

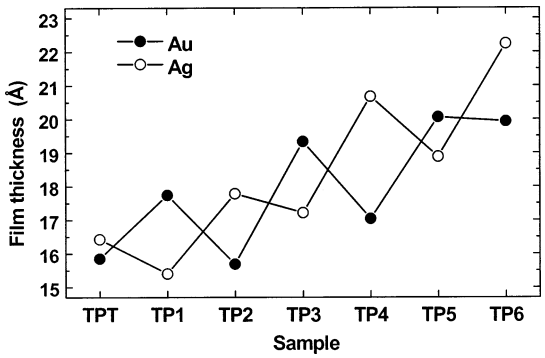

Figure 3. Effective thickness of TP*n*/Au (full circles) and TP*n*/Ag (hollow circles) derived from the ellipsometry data.

TP*n*/Ag, the general behavior is the same as found in the XPS data: There are pronounced zigzag changes in the effective thickness imposed onto the general thickness increase with *n*. The extent of the zigzag change is 10−15% (peak-to-peak), with the direction of the change opposite for TP*n*/Au and TP*n*/Ag.

3.3. IRRAS. The IRRAS spectra of the TP*n* films exhibit the characteristic absorption bands of the aliphatic and aromatic moieties. As an example, some selected regions of the IRRAS spectra of TP*n*/Ag are presented in Figure 4 (the spectra of TP*n*/Au exhibit similar absorption structure). The spectra in the left panel of Figure 4 reveal the symmetric and asymmetric CH_2-stretching vibrations and the C−H stretching vibrations of the terphenyl moiety. The spectra in the middle and right panels of Figure 4 reveal two characteristic C═C stretching modes of the terphenyl moiety. The assignment and position of the adsorption modes in TP*n*/Au and TP*n*/Ag are given in Table 1, where the data for the bulk TP1 compound, TPT, and C16 SAMs on Au are also given (the bulk spectra were recorded using KBr pellets). The intensities of some characteristic modes are presented in Figure 5.

As seen in Table 1, the positions of the symmetric and asymmetric CH_2-stretching vibrations in the TP*n* SAMs are almost the same as those in the well-ordered C16 film and very close to the values observed for crystalline polymethylene chain, which are 2850 and 2920 cm^{-1}, respectively.[49] This implies that the aliphatic linker in the TP*n* film have a crystalline-like structure similar to long-chain alkanethiolate SAMs, i.e., that the linker are predominantly in a planar all-trans conformation.[48] The intensity of the CH_2-stretching vibrations exhibit a steady increase with increasing *n* as expected from the molecular composition in the TP*n* films (see the left panels in Figure 5). In addition, there are slight "odd−even" variations with *n* in the intensity, suggesting that the orientation of the aliphatic linkers might change with varying *n*. The extent of the observed

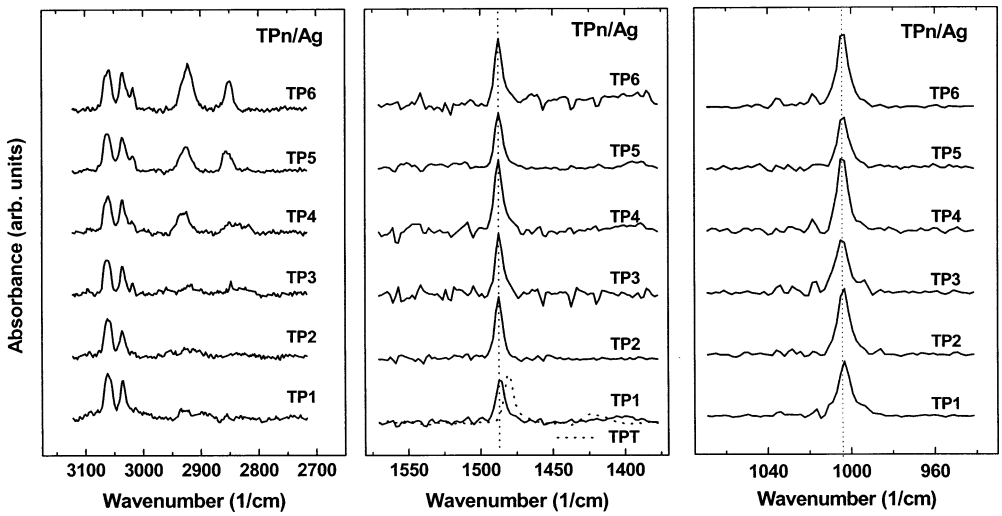

Figure 4. IRRAS spectra of TP*n*/Ag. See Table 1 for the assignment of the absorption bands.

TABLE 1: Assignments and Positions of the Characteristic IR Adsorption Modes in TP*n*/Au and TP*n*/Ag

	band position (cm^{-1})			
mode assignment[a]	TP*n*/Au[b]	TP*n*/Ag[b]	TP1 KBr[c]	TPT or C16 on Au
C═C ring ip	1003.6; 1003.9[d]	1003.2; 1004.0[d]	1002	1002 (TPT)
C═C ring ip	1486.4; 1487.4[d]	1486.4; 1487.4[d]	1482	1478 (TPT)
symmetric C—H stretch[e]	2848	2849.5		2850.5 (C16)
asymmetric C—H stretch[e]	2919	2922		2919 (C16)
═C—H ring	3034.7; 3035.2[d]	3035.6	3031	3037.3 (TPT)
═C—H ring	3059.7; 3060.7[d]	3060.3; 3061.0[d]	3054	3061.6 (TPT)

[a] The mode assignment is performed in accordance with refs 7, 26, and 48. [b] There is no systematic variation in the band position by going from TP1 to TP6. [c] The values for TP1 bulk (KBr) are taken from ref 26. [d] The first value is for $n = 1$, the second for $n = 2-6$. [e] The position of these modes could only be exactly determined for TP4, TP5, and TP6.

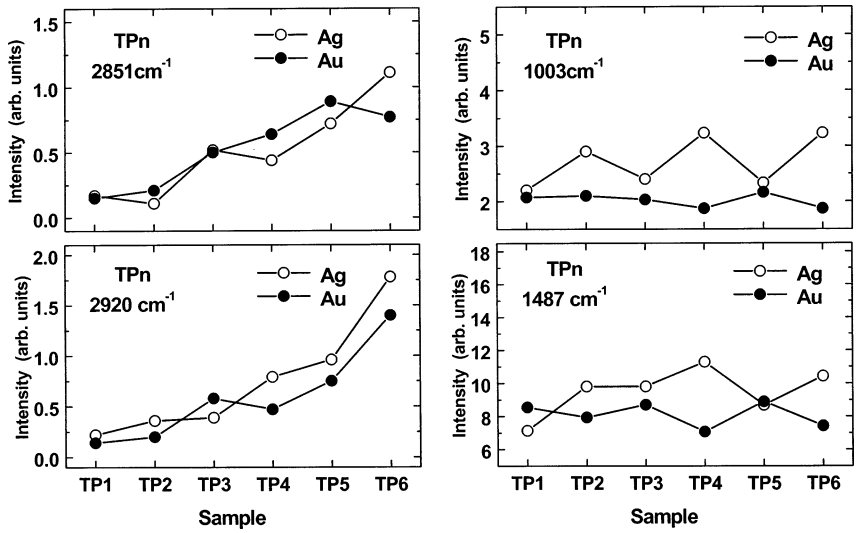

Figure 5. Intensities of the characteristic absorption bands for the C—H stretching modes (left panels) and C═C ring modes (right panels) in TP*n*/Au (full circles) and TP*n*/Ag (hollow circles).

variations is, however, within the accuracy of the IRRAS measurements, so that no unequivocal conclusion on the orientational changes of the aliphatic linker can be derived.

The positions of all characteristic C═C and ═C—H vibrations of the aromatic rings in TP*n*/Au and TP*n*/Ag are shifted to slightly lower values as compared to the KBr spectra. According to the analysis of ref 26, this implies that the TP*n* films exhibit a crystallinity comparable to the bulk materials. In addition, a comparison of the KBr spectrum of TP1[26] with those of the TP*n* SAMs suggests an upright orientation of the terphenyl moieties, because the out-of-plane IR modes of the aromatic rings are hardly visible in the film spectra. The intensities of the in-plane IR-active modes (only such modes are listed in Table 1) in the TP*n* films exhibit pronounced zigzag variation, as, e.g., seen in the right panels of Figure 5, where the *n*-dependence of the intensity of the C═C ring stretching modes is presented. The observed zigzag changes are inverse for Au and Ag substrates. In particular, a higher intensity is observed for odd numbers of the methylene units in TP*n*/Au and even numbers of these entities in TP*n*/Ag. A higher intensity implies a more upright orientation of the terphenyl moieties.

3.4. NEXAFS Spectroscopy. A typical C K-edge NEXAFS spectrum of a TP*n* SAM (taking TP5/Ag as an example) is presented in Figure 6. Individual absorption resonances and the

TABLE 2: Assignments and Positions of the Characteristic NEXAFS Resonances in TP*n*/Au and TP*n*/Ag

resonance assignment[a]	π_1*	R*/C−S*	R*	π_2*	σ_1*	σ_2*	σ_3*
resonance position[b] (eV)	284.95	286.8	287.8	288.8	292.9	299.5	304.4

[a] The resonance assignment is performed in accordance with refs 20, 26, 38, and 45. [b] There is no noticeable variation in the resonance position among the TP*n* films.

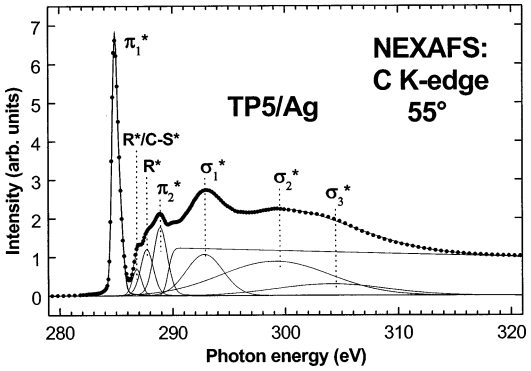

Figure 6. Carbon K-edge NEXAFS spectra of TP5/Ag acquired at X-ray incident angles of 55° (full circles) together with the respective fit (solid line). Individual absorption resonances and the C 1s → continuum edge are shown.

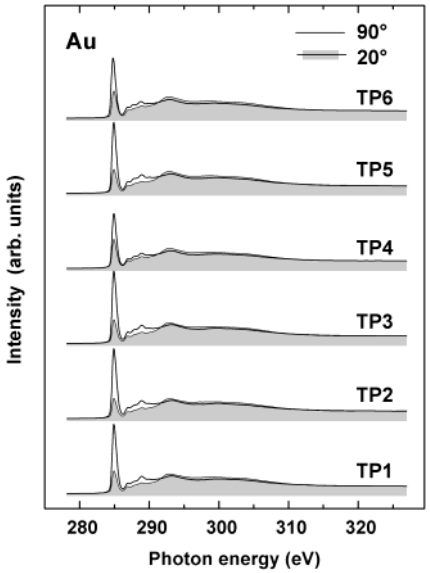

Figure 7. Carbon K-edge NEXAFS spectra of TP*n*/Au acquired at X-ray incident angles of 90° and 20° (shadowed), respectively.

C 1s → continuum edge are shown as well. The assignments and positions of these resonances are given in Table 2. The spectra are dominated by the intense π_1* resonance of the phenyl rings, whereas the R* resonance characteristic for the aliphatic chains is only visible as a shoulder at 287.8 eV. The intensity of this resonance depends on the length of the aliphatic chain.[39,50]

The NEXAFS spectra of TP*n*/Au and TP*n*/Ag exhibit a pronounced linear dichroism (i.e., a dependence of the absorption resonance intensity on the incidence angle of the X-rays), as illustrated by Figures 7 and 8, in which the spectra acquired at X-ray incidence angles of 90° and 20° are presented for TP*n*/Au and TP*n*/Ag, respectively. This indicates an orientational order in the TP*n* SAMs. Considering that the intensity of the π_1* and π_2* resonances is larger at normal than at grazing incidence, an upright orientation of the terphenyl moieties in the TP*n* films can be concluded (the transition dipole moment of the π* resonances is directed perpendicular to the phenyl ring). Along with this general trend, the difference in the intensity of the π* resonances for normal and grazing incidence

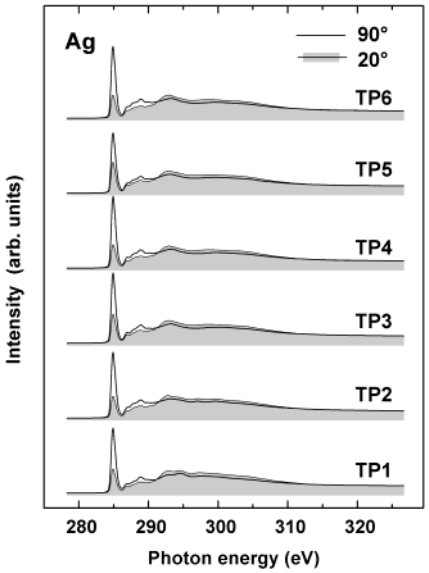

Figure 8. Carbon K-edge NEXAFS spectra of TP*n*/Ag acquired at X-ray incident angles of 90° and 20° (shadowed), respectively.

exhibit a systematic zigzag variation with *n*. This suggests a systematic variation of the orientation of the terphenyl moieties in the TP*n* films from TP1 to TP6. Note that the respective changes in the orientation are opposite for TP*n*/Au and TP*n*/Ag, as follows from a direct comparison of Figure 7 and Figure 8.

The orientation of the terphenyl moieties can be determined from the NEXAFS spectra. For this evaluation, the π_1* resonance has been selected as the most intense absorption feature in the spectra. For an assumed planar conformation of the terphenyl moieties in the TP*n* films (the dihedral angle is equal to zero),[29,51] the average tilt angle φ of the molecular axis of the terphenyl moiety is given by[38,52]

$$I(\theta,\vartheta,\varphi) \propto 1 + \frac{1}{2}(3\cos^2\theta - 1)(3\cos^2\vartheta\sin^2\varphi - 1) \quad (1)$$

where θ is an X-ray incidence angle and ϑ is the twist angle of the aromatic rings with respect to the plane spanned by the surface normal and the molecular axis. Assuming a herringbone arrangement of TPT molecules such as in the bulk materials and aromatic SAMs on Au,[29,41,53] one finds two possible spatial orientations of the biphenyl moieties with reverse twist angles $\vartheta_1 = -\vartheta_2$, but the same tilt angles $\varphi_1 = \varphi_2$. In this case, the contributions of each spatial orientation to the resonance intensity $I(\theta,\vartheta,\varphi)$ are the same and eq 1 can be used for the data evaluation without any modification. Note that a herringbone structure of the aromatic moieties optimizes the intermolecular interaction in the densely packed 2D-layers.

To avoid normalization problems, not the absolute intensities but the intensity ratios $I(\theta)/I(20°)$ were analyzed.[38] In addition, a twist angle of 32° was assumed, as found for thioaromatic bulk materials.[54−57] This assumption is based on theoretical estimates for the molecular arrangements in biphenyl and naphthalene mercaptan films on Au[41] and on the experimental data for a series of oligo(phenylethynyl)benzenethiols.[53] As an example, the angular dependencies of the π_1* resonance

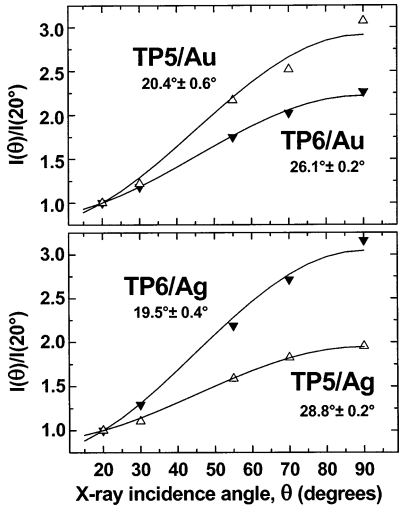

Figure 9. Angular dependence of the π_1* resonance intensity ratio $I(\theta)/I(20°)$ for the TP5 (hollow up triangles) and TP6 (full down triangles) SAMs on Au (upper panel) and Ag (bottom panel) along with the best theoretical fits (solid line). The values of the derived average tilt angle of the terphenyl moieties in the TP*n* films are given at the respective fits.

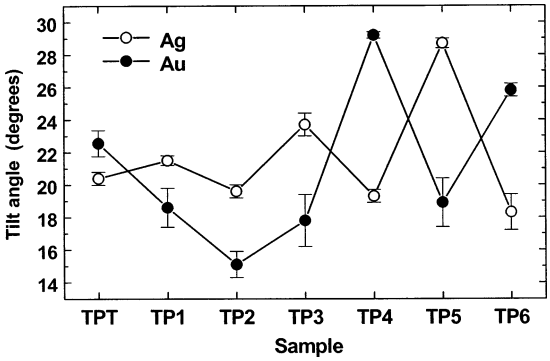

Figure 10. Average tilt angle of the terphenyl moieties in TP*n*/Au (full circles) and TP*n*/Ag (hollow circles) derived from the NEXAFS data. The error bars represent the accuracy of the theoretical fit and are not representative for the accuracy of the NEXAFS experiment, which is usually believed to be ±3−5°.

intensity ratio $I(\theta)/I(20°)$ for the TP5 and TP6 SAMs on Au and Ag are presented in Figure 9, together with the best theoretical fits based on expression (1).

This analysis was performed for all TP*n* films. The derived average tilt angles of the terphenyl moieties are presented in Figure 10. With the only exception of TP2/Au, the average tilt angles exhibit a systematic zigzag variation from TP1 to TP6, with the direction of the respective changes being opposite for Au and Ag. Note that the value for TP2/Au has been verified several times, so that its deviation from the general behavior can be considered as a reliable experimental result. Note also that the low intensity of the R* resonance did not allow us to analyze the orientation of the aliphatic linkers in the TP*n* SAMs.

3.5. Contact Angle Measurements. The advancing and receding water contact angles of the TP*n* films are presented in Figure 11. Both advancing and receding angles are noticeably higher than, e.g., the analogous values for SAMs of 4-mercaptobiphenyl on Au, which are 73° and 69°, respectively.[58] This implies a dense molecular packing of the TP*n* moieties in the respective SAMs. In addition, the difference between the advancing and receding contact angles, i.e., the contact angle hysteresis, is only 11°, which suggests that the film-ambient interface of the TP*n* SAMs is rather smooth. Generally, the

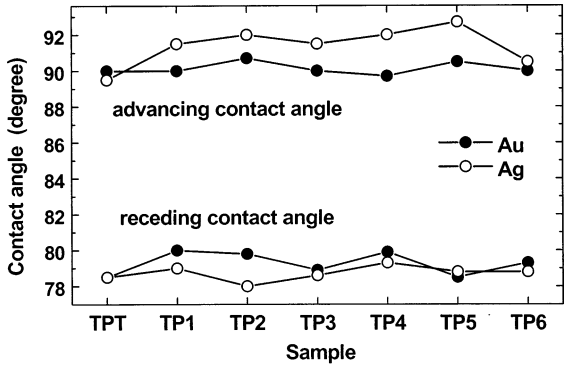

Figure 11. Advancing and receding water contact angles of TP*n*/Au (full circles) and TP*n*/Ag (hollow circles).

contact angle hysteresis in SAMs is about 20°, if no special care is taken to reduce the roughness of the substrate.[58]

For both the advancing and receding water contact angle, the values exhibit slight variations, which assume that the wetting properties of the TP*n* films may change slightly with varying *n*. However, because the extent of these variations is close to the accuracy of the contact angle measurements, no unambiguous conclusions can be derived.

4. Discussion

The results of the XPS, HRXPS, ellipsometry, IRRAS, NEXAFS spectroscopy, and contact angle measurements give a consistent model for the SAMs. Well-defined, densely packed, and contamination-free SAMs of TP*n* have been fabricated on the polycrystalline Au(111) and Ag(111) substrates. Though the XPS and HRXPS S 2p spectra are consistent with a thiolate-like bonding of the TP*n* molecules to the substrates, the XPS and HRXPS C 1s spectra, IR spectra, and NEXAFS spectra exhibit the respective emission and absorption bands for intact alkyl and terphenyl moieties in the TP*n* films. The general dependence of the intensity of these spectral features follows exactly the molecular composition of the TP*n* molecules: Whereas the features related to the aliphatic part exhibit a steady intensity increase with *n*, the features related to the aromatic part remain generally constant by going from TP1 to TP6 for both Au and Ag substrates.

Imposed onto these general trends, we observe pronounced and systematic odd−even effects with respect to the number *n* of the methylene units in the aliphatic linker. The packing density of the TP*n* films exhibit an odd−even variation by 10−15% (peak-to-peak), as implied by the XPS, HRXPS, and ellipsometry data. These changes in the packing density are accompanied by respective odd−even changes in the orientation of the SAM constituents. As follows from the IRRAS and NEXAFS data, the average tilt angle of the terphenyl moieties in TP*n*/Au and TP*n*/Ag exhibits odd−even variation by 7−14°. With the only exception of TP2/Au, the respective changes in the tilt angle correlate perfectly with the changes in the packing density: a higher packing density is observed for a smaller tilt angle of the terphenyl moieties and vice versa. The experimental data do not allows us to make an equivocal conclusion on odd−even changes in the orientation of the aliphatic spacers, but only on their conformation, which is similar to that in long-chain AT SAMs. It seems that there are odd−even effects, but with a rather small amplitude. The same conclusion applies to the wetting properties of the TP*n* SAMs; i.e., the odd−even changes in the orientation and packing density of the SAM constituents do not result in pronounced changes in the wetting properties.

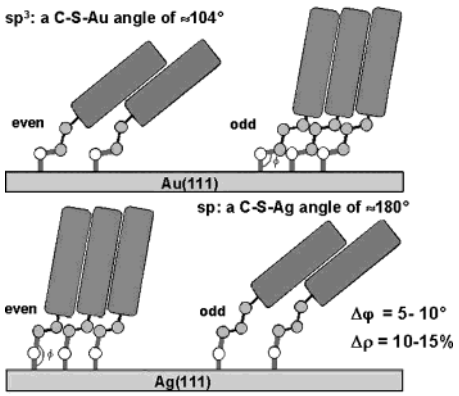

Figure 12. Schematic drawing of the orientation and packing of the TP*n* molecules in the respective SAMs on Au and Ag.

All observed odd−even effects are opposite on Au as compared to Ag. A higher packing density and a smaller inclination of the terphenyl moieties is observed for an odd number of the methylene units in the aliphatic linker of TP*n*/Au, and an even number of these units for TP*n*/Ag. Vice versa, a lower packing density and a larger inclination of the terphenyl moieties was found for an even number of the methylene units in the aliphatic linker of TP*n*/Au and an odd number of these units for TP*n*/Ag.

The odd−even effects in the TP*n* films are very similar to those in the BPn SAMs[17,19] (see section 1), in both their dependence on *n* and their extent, even though the latter appear to be somewhat weaker comparing to the BPn films. These effects can be consistently explained by assuming that the character the headgroup-substrate bond in SAMs of alkanethiols is an important parameter affecting the packing density and molecular orientation of the SAM constituents. This is illustrated by a schematic drawing in Figure 12. Assuming an sp^3 hybridization of the thiolate headgroups on Au (a substrate-S−C angle of ≈104°) and a rigid aliphatic linker in all-trans conformation (as shown by IRRAS), one gets a less tilted orientation of the terphenyl moieties in TP*n*/Au for an odd *n* and a more tilted orientation for an even *n*. Contrary, in the case of an sp hybridization of the thiolate headgroup on Ag (a substrate-S−C angle of ≈180°), a less tilted orientation of the terphenyl moieties in TP*n*/Ag is realized for an even *n* and a less tilted one for an odd *n*. The true substrate−S−C angles in the TP*n* SAMs are probably not exactly equal to ≈104° and ≈180°, but rather the respective bending potentials depend on the deviation of the metal−S−C angle from these optimal values and hence contribute to the overall balance of the structural forces. Both for the BPn and TP*n* SAMs, this contribution obviously prevails over intermolecular forces, which results in the formation of the "loosely-packed" layers (at even *n* on Au and odd *n* on Ag, respectively), which are unfavorable from the viewpoint of optimized chain-chain interaction. The addition of one more phenyl ring by going from BPn to TP*n* resulted neither in the disappearance nor in a significant decrease in the extent of the odd−even effects.

The only exception from the general trend is found in the TP2/Au NEXAFS data. Whereas the packing density of this SAM follows the general trend of the other TP*n* films, the average tilt angle of the terphenyl moieties was found to be noticeably smaller than the value expected for the odd−even behavior. We assume, that for this particular film a special arrangement of the SAM constituents occur, which could be, e.g., related to a different twist angle of the terphenyl moieties than assumed in the numerical analysis of the NEXAFS data. As shown in recent STM studies of BPn SAMs, the exact structure of these films can be noticeably different for different odd or even *n*, even though there are some common features.[21,59]

In conclusion, one more difference between the BPn and TP*n* systems has to be mentioned, namely the lack or a very small extent of the odd−even effect in the water contact angle in the latter case. We believe that this difference is related to the different termination of the BPn and TP*n* molecules, namely to the absence of the methyl end group in the case of TP*n*.

5. Conclusion

The packing density and orientational and conformational order of 4,4′-terphenyl-substituted alkanethiolate SAMs on polycrystalline (111) gold and silver substrates were studied by XPS, HRXPS, ellipsometry, IRRAS, NEXAFS spectroscopy, and water contact angle measurements. The SAMs were found to be well-defined, densely packed, and contamination free.

The packing density and the orientation of the terphenyl moieties in the TP*n* SAMs exhibited a pronounced zigzag variation with *n* from TP1 to TP6, which was opposite on silver than on gold. A higher packing density and a smaller inclination of the terphenyl moieties was observed for an odd number of the methylene units in the aliphatic linker in TP*n*/Au, and an even number of these units in TP*n*/Ag. Vice versa, a lower packing density and a larger inclination of the terphenyl moieties was found for an even number of the methylene units in the aliphatic linker in TP*n*/Au, and an odd number of these units in TP*n*/Ag.

The observed odd−even effects can be explained by assuming that the bending potentials of the substrate−S−C entity depends strongly on the deviation of the metal−S−C bonding angle from an optimal value of ≈104° (Au) and ≈180° (Ag), respectively. The optimal substrate−S−C angles are associated with the bonding configurations of the sulfur headgroups, which are assumed to have an sp^3 hybridization on Au and an sp hybridization on Ag, respectively.

The odd−even effects in the TP*n* films are very similar to those observed previously in SAMs of biphenyl-substituted alkanethiols on Au and Ag,[17,19,21] both in their dependence on *n* and in their extent (even though the effects appear to be somewhat weaker comparing to the BPn films). This suggests a common origin of the observed phenomena in all alkanethiolate SAMs, which we identify as the role of the headgroup−substrate bond in the balance of structural forces, which determine the packing density and molecular orientation in these systems. Both for the BPn and TP*n* SAMs, the rigidity of the metal−S−C bending potentials obviously dominates over the intermolecular forces.

An exact knowledge of all factors affecting the structure in monomolecular films is an important prerequisite for molecular engineering of SAMs and applications of these systems. A practical example has been reported recently, i.e., that the radiation sensitivity of monomolecular resists can be tailored by the variation in the packing density of its molecular constituents.[60]

Acknowledgment. We thank Ch. Wöll (Universität Bochum) for providing the experimental equipment for the NEXAFS measurements, L. S. O. Johansson (Karlstad University) for the cooperation at MAX-lab, and the BESSY II and MAX-lab staff for the assistance during the synchrotron-based experiments. This work has been supported by the German BMBF (GRE1HD), Deutsche Forschungsgemeinschaft (JA 883/4-2), Access to

Research Infrastructure action of the Human Potential Program of the European Community, and the Fonds der Chemischen Industrie.

References and Notes

(1) Ulman, A. *An Introduction to Ultrathin Organic Films: Langmuir−Blodgett to Self-Assembly*; Academic Press: New York, 1991.
(2) Ulman, A. *Chem. Rev.* **1996**, *96*, 1533.
(3) *Thin films: self-assembled monolayers of thiols*; Ulman A., Ed.; Academic Press: San Diego, CA, 1998.
(4) Schreiber, F. *Prog. Surf. Sci.* **2000**, *65*, 151.
(5) Frey, S.; Shaporenko, A.; Zharnikov, M.; Harder, P.; Allara, D. L. *J. Phys. Chem. B* **2003**, *107*, 7716.
(6) Bain, C. D.; Troughton, E. B.; Tao, Y.-T.; Evall, J.; Whitesides, G. M.; Nuzzo, R. G. *J. Am. Chem. Soc.* **1989**, *111*, 321.
(7) Nuzzo, R. G.; Dubois, L. H.; Allara, D. L. *J. Am. Chem. Soc.* **1990**, *112*, 558.
(8) Laibinis, P. E.; Whitesides, G. M.; Allara, D. L.; Tao, Y.-T.; Parikh, A. N.; Nuzzo, R. G. *J. Am. Chem. Soc.* **1991**, *113*, 7152.
(9) Sellers, H.; Ulman, A.; Shnidman, Y.; Eilers, J. E. *J. Am. Chem. Soc.* **1993**, *115*, 9389.
(10) Ulman, A.; Eilers, J. E.; Tillman, N. *Langmuir* **1989**, *5*, 1147.
(11) Fenter, P.; Eisenberger, P.; Li, J.; Camillone, N., III; Bernasek, S.; Scoles, G.; Ramanarayanan, T. A.; Liang, K. S. *Langmuir* **1991**, *7*, 2013.
(12) Rieley, H.; Kendall, G. K.; Jones, R. G.; Woodruff, P. *Langmuir* **1999**, *15*, 8856.
(13) Fenter, P.; Eisenberger, P.; Liang, K. S. *Phys. Rev. Lett.* **1993**, *70*, 2447; Fenter, P.; Eberhardt, A.; Eisenberger, P. *Science* **1994**, *266*, 1216.
(14) Poirier, G. E.; Tarlov, M. J. *Langmuir* **1994**, *10*, 2853.
(15) Thome, J.; Himmelhaus, M.; Zharnikov, M.; Grunze, M. *Langmuir* **1998**, *14*, 7435.
(16) Walczak, M. M.; Chung, C.; Stole, S. M.; Widrig, C. A.; Porter, M. D. *J. Am. Chem. Soc.* **1991**, *113*, 2370.
(17) Zharnikov, M.; Frey, S.; Rong, H.; Yang, Y. J.; Heister, K.; Buck, M.; Grunze, M. *Phys. Chem. Chem. Phys.* **2000**, *2*, 3359.
(18) Frey, S.; Heister, K.; Zharnikov, M.; Grunze, M., Tamada, K.; Colorado, R., Jr.; Graupe, M.; Shmakova, O. E.; Lee, T. R. *Isr. J. Chem.* **2000**, *40*, 81.
(19) Rong, H. T.; Frey, S.; Yang, Y. J.; Zharnikov, M.; Buck, M.; Wühn, M.; Wöll, Ch.; Helmchen, G. *Langmuir* **2001**, *17*, 1582.
(20) Zharnikov, M.; Grunze, M. *J. Phys. Condens. Matter.* **2001**, *13*, 11333.
(21) Azzam, W.; Cyganik, P.; Witte, G.; Buck, M.; Wöll, Ch. *Langmuir* **2003**, *19*, 8262.
(22) Ishida, T.; Choi, N.; Mizutani, W.; Tokumoto, H.; Kojima, I.; Azehara, H.; Hokari, H.; Akiba, U.; Fujihira, M. *Langmuir* **1999**, *15*, 6799.
(23) Ishida, T.; Mizutani, W.; Akiba, U.; Umemura, K.; Inoue, A.; Choi, N.; Fujihira, M.; Tokumoto, H. *J. Phys. Chem. B* **1999**, *103*, 1686.
(24) Ishida, T.; Mizutani, W.; Choi, N.; Akiba, U.; Fujihira, M.; Tokumoto, H. *J. Phys. Chem. B* **2000**, *104*, 11680.
(25) Ishida, T.; Mizutani, W.; Tokumoto, H.; Choi, N.; Akiba, U.; Fujihira, M. *J. Vac. Sci. Technol. A* **2000**, *18*, 1437.
(26) Fuxen, C.; Azzam, W.; Arnold, R.; Witte, G.; Terfort, A.; Wöll, Ch. *Langmuir* **2001**, *17*, 3689.
(27) Arnold, R.; Azzam, W.; Terfort, A.; Wöll, Ch. *Langmuir* **2002**, *18*, 3980.
(28) Ishida, T.; Mizutani, W.; Aya, Y.; Ogiso, H.; Sasaki, S.; Tokumoto, H. *J. Phys. Chem. B* **2002**, *106*, 5886.
(29) Himmel, H.-J.; Terfort, A.; Wöll, Ch. *J. Am. Chem. Soc.* **1998**, *120*, 12069.
(30) Brunnbauer, M. Ph.D. Thesis, Universität Hamburg, 2003.
(31) Köhn, F. Diploma Thesis, Universität Heidelberg, Heidelberg, Germany, 1998.
(32) Heister, K.; Zharnikov, M.; Grunze, M.; Johansson, L. S. O. *J. Phys. Chem. B* **2001**, *105*, 4058.
(33) Wirde, M.; Gelius, U.; Dunbar, T.; Allara, D. L. *Nucl. Instrum. Methods Phys. Res. B* **1997**, *131*, 245.
(34) Jäger, B.; Schürmann, H.; Müller, H. U.; Himmel, H.-J.; Neumann, M.; Grunze, M.; Wöll, Ch. *Z. Phys. Chem.* **1997**, *202*, 263.
(35) Heister, K.; Zharnikov, M.; Grunze, M.; Johansson, L. S. O.; Ulman, A. *Langmuir* **2001**, *17*, 8.
(36) Zharnikov, M.; Grunze, M. *J. Vac. Sci. Technol. B* **2002**, *20*, 1793.
(37) Moulder, J. F.; Stickle, W. E.; Sobol, P. E.; Bomben, K. D. In *Handbook of X-ray Photoelectron Spectroscopy*; Chastian, J., Ed.; Perkin-Elmer Corp.: Eden Prairie, MN, 1992.
(38) Stöhr, J. *NEXAFS Spectroscopy*; Springer Series in Surface Science 25; Springer-Verlag: Berlin, 1992.
(39) Zharnikov, M.; Frey, S.; Heister, K.; Grunze, M. *Langmuir* **2000**, *16*, 2697.
(40) Batson, P. E. *Phys. Rev. B* **1993**, *48*, 2608.
(41) Chang, S.-C.; Chao, I.; Tao, Y.-T. *J. Am. Chem. Soc.* **1994**, *116*, 6792.
(42) Gölzhäuser, A.; Panov, S.; Schertel, A.; Mast, M.; Wöll, Ch.; Grunze, M. *Surf. Sci.* **1995**, *334*, 235.
(43) Whelan, C. M.; Barnes, C. J.; Walker, C. G. H.; Brown, N. M. D. *Surf. Sci.* **1999**, *425*, 195.
(44) Whelan, C. M.; Smyth, M. R.; Barnes, C. J. *Langmuir* **1999**, *15*, 116.
(45) Frey, S.; Stadler, V.; Heister, K.; Eck, W.; Zharnikov, M.; Grunze, M.; Zeysing, B.; Terfort, A. *Langmuir* **2001**, *17*, 2408.
(46) Heister, K.; Rong, H.-T.; Buck, M.; Zharnikov, M.; Grunze, M.; Johansson, L. S. O. *J. Phys. Chem. B* **2001**, *105*, 6888.
(47) A detailed discussion of the HRXPS spectra will be published elsewhere.
(48) Porter, M. D.; Bright, T. B.; Allara, D. L.; Chidsey, C. E. D. *J. Am. Chem. Soc.* **1987**, *109*, 3559.
(49) Snyder, R. G.; Strauss, H. L.; Elliger, C. A. *J. Phys. Chem.* **1982**, *86*, 5145.
(50) Hähner, G.; Kinzler, M.; Thümmler, C.; Wöll, Ch.; Grunze, M. *J. Vac. Sci. Technol.* **1992**, *10*, 2758.
(51) Lii, J.-H.; Allinger, N. L. *J. Am. Chem. Soc.* **1989**, *111*, 8576.
(52) Shaporenko, A.; Adlkofer, K.; Johansson, L. S. O.; Tanaka, M.; Zharnikov, M. *Langmuir* **2003**, *19*, 4992.
(53) Dhirani, A.-A.; Zehner, W.; Hsung, R. P.; Guyot-Sionnest, P.; Sita, L. *J. Am. Chem. Soc.* **1996**, *118*, 3319.
(54) Cruickshank, D. W. J. *Acta Crystallogr.* **1956**, *9*, 915.
(55) Kitaigorodskii, I. A. *Organic Chemical Crystallography*; Consultants Bureau: New York, 1961.
(56) Trotter, J. *Acta Crystallogr.* **1961**, *14*, 1135.
(57) Charbonneau, G.-P.; Delugeard, Y. *Acta Crystallogr.* **1976**, *B32*, 1420.
(58) Kang, J. F.; Ulman, A.; Liao, S.; Jordan, R.; Yang, G.; Liu, G-yu *Langmuir* **2001**, *17*, 95.
(59) Cyganik, P.; Buck, M.; Azzam, W.; Wöll, Ch. *J. Phys. Chem. B*, in press.
(60) Frey, S.; Rong, H.-T.; Heister, K.; Yang, Y.-J.; Buck, M.; Zharnikov, M. *Langmuir* **2002**, *18*, 3142.